15

Porosome

The Fusion Pore Revealed by Multiple Imaging Modalities

Bhanu P. Jena

Summary

Secretion occurs in all cells of multicellular organisms and involves the delivery of secretory products packaged in membrane-bound vesicles to the cell exterior. Specialized cells for neurotransmission, enzyme secretion, or hormone release utilize a highly regulated secretory process. Secretory vesicles are transported to specific sites at the plasma membrane, where they dock and fuse to release their contents. Similar to other cellular processes, cell secretion is found to be highly regulated and a precisely orchestrated event. It has been demonstrated that membrane-bound secretory vesicles dock and fuse at porosomes, which are specialized supramolecular structures at the cell plasma membrane. Swelling of secretory vesicles results in a buildup of pressure, allowing expulsion of intravesicular contents. The extent of secretory vesicle swelling dictates the amount of intravesicular contents expelled during secretion. The discovery of the porosome, its isolation, its structure and dynamics at nanometer resolution and in real time, and its biochemical composition and functional reconstitution into artificial lipid membrane have been determined. The molecular mechanism of secretory vesicle fusion at the base of porosomes and vesicle swelling have also been resolved. These findings reveal the molecular machinery and mechanism of cell secretion. In this chapter, the discovery of the porosome, its isolation, its structure and dynamics at nanometer resolution and in real time, and its biochemical composition and functional reconstitution into artificial lipid membrane are discussed.

Key Words: Fusion pore; atomic force microscopy; electron microscopy.

1. Introduction

Secretion and membrane fusion are fundamental cellular processes regulating endoplasmic reticulum-Golgi transport, plasma membrane recycling, cell division, sexual reproduction, acid secretion, and the release of enzymes, hormones, and neurotransmitters, to name just a few. It is, therefore, no surprise that defects in secretion and membrane fusion give rise to diseases like diabetes,

From: *Methods in Molecular Biology, vol. 319: Cell Imaging Techniques: Methods and Protocols*
Edited by: D. J. Taatjes and B. T. Mossman © Humana Press Inc., Totowa, NJ

Alzheimer's, Parkinson's, acute gastroduodenal diseases, gastroesophageal reflux disease, intestinal infections due to inhibition of gastric acid secretion, biliary diseases resulting from malfunction of secretion from hepatocytes, polycystic ovarian disease as a result of altered gonadotropin secretion, and Gitelman disease associated with growth hormone deficiency and disturbances in vasopressin secretion are only a few examples. Understanding cellular secretion and membrane fusion helps not only to advance our understanding of these vital cellular and physiological processes, but in the development of drugs also to help ameliorate secretory defects, provide insight into our understanding of cellular entry and exit of viruses and other pathogens, and in the development of smart drug delivery systems. Therefore, secretion and membrane fusion play an important role in health and disease. Studies *(1–21),* in the last decade demonstrate that membrane-bound secretory vesicles dock and transiently fuse at the base of specialized plasma membrane structures called porosomes or fusion pores, to expel vesicular contents. These studies further demonstrate that during secretion, secretory vesicles swell, enabling the expulsion of intravesicular contents through porosomes *(16,19–21)*. With these findings *(1–21)*, a new understanding of cell secretion has emerged and confirmed by a number of laboratories *(22–27)*.

Throughout history, the development of new imaging tools has provided new insights into our perceptions of the living world and profoundly impacted human health. The invention of the light microscope almost 300 yr ago was the first catalyst, propelling us into the era of modern biology and medicine. Using the light microscope, a giant step into the gates of modern medicine was made by the discovery of the unit of life—the cell. The structure and morphology of normal and diseased cells and of disease-causing microorganisms were revealed for the first time using the light microscope. Then, in 1938, with the birth of the electron microscope (EM), dawned a new era in biology and medicine. Through the mid-1940s and 1950s, a number of subcellular organelles were discovered and their functions determined using the EM. Viruses, the new life-forms were discovered and observed for the first time and implicated in diseases ranging from the common cold to acquired immune disease (aquired immune deficiency syndrome [AIDS]). Despite the capability of the EM to image biological samples at near-nanometer resolution, sample processing (fixation, dehydration, staining) results in morphological alterations and was a major concern. Then, in the mid-1980s, scanning probe microscopy evolved *(1,28)*, further extending our perception of the living world to the near-atomic realm. One such scanning probe microscope, the atomic force microscope (AFM), has helped overcome both limitations of light and electron microscopy, enabling determination of the structure and dynamics of single biomolecules and live cells in three dimensions, at

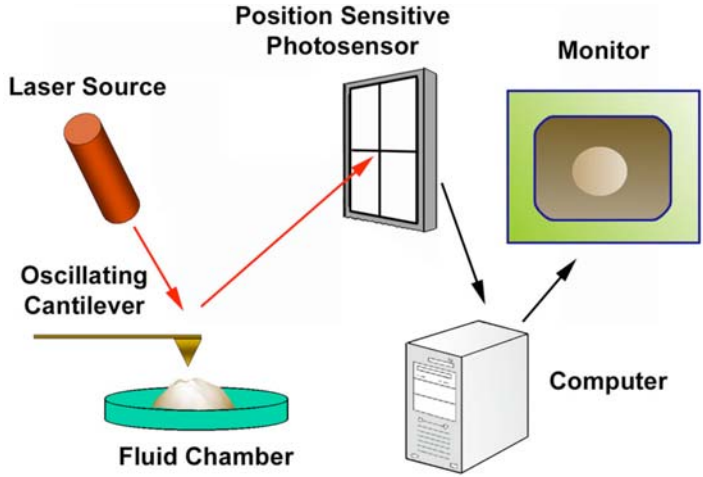

Fig. 1. Schematic diagram depicting key components of an atomic force microscope. (From **ref.** *12*.)

near-angstrom resolution. This unique capability of the AFM has given rise to a new discipline of "nanobioscience," heralding a new era in biology and medicine. Using AFM in combination with conventional tools and techniques, this past decade has witnessed advances in our understanding of cell secretion *(1–21)* and membrane fusion *(9,17,18,29)*, as noted earlier in the chapter.

The resolving power of the light microscope is dependent on the wavelength of the light used and, therefore, 250–300 nm in lateral and much less in depth resolution can be achieved at best. The porosome or fusion pore in live secretory cells are cup-shaped structures, measuring 100–150 nm at its opening and 15–30 nm in relative depth in the exocrime pancreas, and just 10 nm at the presynaptic membrane of the nerve terminal. As a result, it had evaded visual detection until its discovery using the AFM *(3–8,15)*. The development of the AFM *(28)* has enabled the imaging of live cells in physiological buffer at nanometer to subnanometer resolution. In AFM, a probe tip microfabricated from silicon or silicon nitride and mounted on a cantilever spring is used to scan the surface of the sample at a constant force. Either the probe or the sample can be precisely moved in a raster pattern using a xyz piezotube to scan the surface of the sample (*see* **Fig. 1**). The deflection of the cantilever, measured optically, is used to generate an isoforce relief of the sample *(30)*. Thus, force is used to image surface profiles of objects by the AFM, allowing imaging of live cells and subcellular structures submerged in physiological buffer solutions. To image live cells, the scanning probe of the AFM operates in physiological

buffers and can do so under two modes: contact or tapping. In the contact mode, the probe is in direct contact with the sample surface as it scans at a constant vertical force. Although high-resolution AFM images can be obtained in this mode of AFM operation, sample height information generated might not be accurate because the vertical scanning force could depress the soft cell. However, information on the viscoelastic properties of the cell and the spring constant of the cantilever enables measurement of the cell height. In the tapping mode, on the other hand, the cantilever resonates and the tip makes brief contacts with the sample. In the tapping mode in fluid, lateral forces are virtually negligible. It is therefore important that the topology of living cells be obtained using both contact and tapping modes of AFM operation in fluid. The scanning rate of the tip over the sample also plays an important role on the quality of the image. Because cells are soft samples, a high scanning rate would influence its shape. Hence, a slow tip movement over the cell would be ideal and results in minimal distortion and better image resolution. Rapid cellular events might be further monitored by using section analysis. To examine isolated cells by the AFM, freshly cleaved mica coated with Cel-Tak has also been used with great success *(3–8)*. Also, to obtain optimal resolution, the contents of the bathing medium as well as the cell surface to be scanned should be devoid of any debris.

2. Methods

2.1. Isolation of Pancreatic Acinar Cells

Acinar cells for secretion experiments, light microscopy, AFM, and EM were isolated using a minor modification of a published procedure. For each experiment, a male Sprague–Dawley rat weighing 80–100 g was euthanized by CO_2 inhalation. The pancreas was dissected and diced into 0.5-mm^3 sections with a razor blade, mildly agitated for 10 min at 37°C in a siliconized glass tube with 5 mL of oxygenated buffer A (98 m*M* NaCl, 4.8 m*M* KCl, 2 m*M* $CaCl_2$, 1.2 m*M* $MgCl_2$, 0.1% bovine serum albumin, 0.01% soybean trypsin inhibitor, 25 m*M* HEPES, pH 7.4) containing 1000 units of collagenase. The suspension of acini was filtered through a 224-µm Spectra-Mesh (Spectrum Laboratory Products, Rancho Dominguez, CA) polyethylene filter to remove large clumps of acini and undissociated tissue. The acini were washed six times, 50 mL per wash, with ice-cold buffer A. Isolated rat pancreatic acini and acinar cells were plated on Cell-Tak-coated (Collaborative Biomedical Products, Bedford, MA) glass cover slips. Two to three hours after plating, cells were imaged with the AFM before and during stimulation of secretion. Isolated acinar cells and hemiacinar preparations were used in the study because fusion of secretory vesicles at the protein membrane (PM) in these cells occurs at the apical region facing the acinar lumen.

2.2. Pancreatic Plasma Membrane Preparation

Rat pancreatic PM fractions were isolated using a modification of a published method. Male Sprague–Dawley rats weighing 70–100 g were euthanized by CO_2 inhalation. The pancreases were removed and placed in ice-cold phosphate-buffered saline (PBS), pH 7.5. Adipose tissue was removed and the pancreases were diced into 0.5-mm^3 pieces using a razor blade in a few drops of homogenization buffer A (1.25 *M* sucrose, 0.01% trypsin inhibitor, and 25 m*M* HEPES, pH 6.5). The diced tissue was homogenized in 15% (w/v) ice-cold homogenization buffer A using four strokes at maximum speed of a motor-driven pestle (Wheaton overhead stirrer). One and a half milliliters of the homogenate was layered over a 125-µL cushion of 2 *M* sucrose and 500 µL of 0.3 *M* sucrose was layered onto the homogenate in Beckman centrifuge tubes. After centrifugation at 145,000*g* for 90 min in a Sorvall AH-650 rotor, the material banding between the 1.2 *M* and 0.3 *M* sucrose interface was collected and the protein concentration was determined. For each experiment, fresh PM was prepared and used the same day in all AFM experiments.

2.2.1. Isolation of Synaptosomes, Synaptosomal Membrane, and Synaptic Vesicles

Synaptosomes, synaptosomal membrane, and synaptic vesicles were prepared from rat brains *(31,32)*. Whole rat brains from Sprague–Dawley rats (100–150 g) were isolated and placed in ice-cold buffered sucrose solution (5 m*M* HEPES, pH 7.4, 0.32 *M* sucrose) supplemented with protease inhibitor cocktail (Sigma, St. Louis, MO) and homogenized using a Teflon–glass homogenizer (8–10 strokes). The total homogenate was centrifuged for 3 min at 2500*g*. The supernatant fraction was further centrifuged for 15 min at 14,500*g*, and the resultant pellet was resuspended in buffered sucrose solution, which was loaded onto 3-10-23% Percoll gradients. After centrifugation at 28,000*g* for 6 min, the enriched synaptosomal fraction was collected at the 10–23% Percoll gradient interface. To isolate synaptic vesicles and synaptosomal membrane *(32)*, isolated synaptosomes were diluted with 9 vol of ice-cold H_2O (hypotonic lysis of synaptosomes to release synaptic vesicles) and immediately homogenized with three strokes in Dounce homogenizer, followed by a 30-min incubation on ice. The homogenate was centrifuged for 20 min at 25,500*g*, and the resultant pellet (enriched synaptosomal membrane preparation) and supernatant (enriched synaptic vesicles preparation) were used in our studies.

2.2.2. Preparation of Lipid Membrane on Mica and Porosome Reconstitution

To prepare lipid membrane on mica for AFM studies, freshly cleaved mica disks were placed in a fluid chamber. Two hundred microliters of the bilayer

bath solution, containing 140 m*M* NaCl, 10 m*M* HEPES, and 1 m*M* $CaCl_2$, were placed at the center of the cleaved mica disk. Ten microliters of the brain lipid vesicles were added to the above bath solution. The mixture was then allowed to incubate for 60 min at room temperature, before washing (10X), using 100 µL bath solution/wash. The lipid membrane on mica was imaged by the AFM before and after the addition of immunoisolated porosomes.

2.3. Atomic Force Microscopy

"Pits" and fusion pores at the PM in live pancreatic acinar secreting cells in PBS, pH 7.5, were imaged with the AFM (Bioscope III, Digital Instruments) using both contact and tapping modes. All images presented in this chapter were obtained in the "tapping" mode in fluid, using silicon nitride tips with a spring constant of 0.06 Nm, and an imaging force of <200 pN. Images were obtained at line frequencies of 1 Hz, with 512 lines per image, and constant image gains. Topographical dimensions of "pits" and fusion pores at the cell PM were analyzed using the software nanoscopeIIIa 4.43r8 supplied by Digital Instruments.

2.4. ImmunoAFM on Live Cells

Immunogold localization in live pancreatic acinar cells was assessed after 5 min stimulation of secretion with 10 µ*M* of the secretagogue mastoparan. After stimulation of secretion, the live pancreatic acinar cells in buffer were exposed to a 1 : 200 dilution of α-amylase-specific antibody (Biomeda Corp., Foster City, CA) and 30 nm colloidal gold-conjugated secondary antibody for 1 min and were washed in PBS before AFM imaging in PBS at room temperature. "Pits" and fusion pores within and at the apical end of live pancreatic acinar cells in PBS, pH 7.5, were imaged by the AFM (Bioscope III, Digital Instruments) using both contact and tapping modes. All images presented were obtained in the "tapping" mode in fluid, using silicon nitride tips as described previously.

2.5. ImmunoAFM on Fixed Cells

After stimulation of secretion with 10 µ*M* mastoparan, the live pancreatic acinar cells were fixed for 30 min using ice-cold 2.5% paraformaldehyde in PBS. Cells were then washed in PBS, followed by labeling with 1 : 200 dilution of α-amylase-specific antibody (Biomeda Corp.) and 10 nm gold-conjugated secondary antibody for 15 min, fixed, washed in PBS, and imaged in PBS with AFM at room temperature.

2.6. Isolation of Zymogen Granules

Zymogen granules (ZGs) were isolated by using a modification of the method of our published procedure. Male Sprague–Dawley rats weighing 80–100 g were

euthanized by CO_2 inhalation for each ZG preparation. The pancreas was dissected and diced into 0.5-mm^3 pieces. The diced pancreas was suspended in 15% (w/v) ice-cold homogenization buffer (0.3 *M* sucrose, 25 m*M* HEPES, pH 6.5, 1 m*M* benzamidine, 0.01% soybean trypsin inhibitor) and homogenized with a Teflon-glass homogenizer. The resultant homogenate was centrifuged for 5 min at 300*g* at 4°C to obtain a supernatant fraction. One volume of the supernatant fraction was mixed with 2 vol of a Percoll–sucrose–HEPES buffer (0.3 *M* sucrose, 25 m*M* HEPES, pH 6.5, 86% Percoll, 0.01% soybean trypsin inhibitor) and centrifuged for 30 min at 16,400*g* at 4°C. Pure ZGs were obtained as a loose white pellet at the bottom of the centrifuge tube.

2.7. Transmission Electron Microscopy

Isolated rat pancreatic acini and ZGs were fixed in 2.5% buffered paraformaldehyde (PFA) for 30 min, and the pellets were embedded in Unicryl resin and were sectioned at 40–70 nm. Thin sections were transferred to coated specimen transmission electron microscope (TEM) grids, dried in the presence of uranyl acetate and methyl cellulose and examined in a TEM.

2.8. Immunoprecipitation and Western Blot Analysis

Immunoblot analysis was performed on pancreatic PM and total homogenate fractions. Protein in the fractions was estimated by the Bradford method. Pancreatic fractions were boiled in Laemmli reducing sample preparation buffer for 5 min, cooled and used for sodium dodecyl sulfate–polyacrylamide gel electrophoresis (SDS-PAGE). PM proteins were resolved in a 12.5% SDS-PAGE and electrotransferred to 0.2-μm nitrocellulose sheets for immunoblot analysis with a SNAP-23 specific antibody. The nitrocellulose was incubated for 1 h at room temperature in blocking buffer (5% nonfat milk in PBS containing 0.1% Triton X-100 and 0.02% NaN_3) and immunoblotted for 2 h at room temperature with the SNAP-23 antibody (ABR, Golden, CO). The primary antibodies were used at a dilution of 1:10,000 in blocking buffer. The immunoblotted nitrocellulose sheets were washed in PBS containing 0.1% Triton X-100 and 0.02% NaN_3 and were incubated for 1 h at room temperature in horseradish peroxidase (HRP)-conjugated secondary antibody at a dilution of 1:2000 in blocking buffer. The immunoblots were then washed in the PBS buffer, processed for enhanced chemiluminescence, and exposed to X-OMAT-AR film. To isolate the fusion complex for immunoblot analysis, SNAP-23 specific antibody conjugated to protein A–Sepharose was used. One gram of total pancreatic homogenate solubilized in Triton/Lubrol solubilization buffer (0.5% Lubrol; 1 m*M* benzamidine; 5 m*M* ATP; 5 m*M* EDTA; 0.5 % Triton X-100, in PBS) supplemented with protease inhibitor mix (Sigma, St. Louis, MO) was

used. SNAP-23 antibody conjugated to the protein A–Sepharose was incubated with the solubilized homogenate for 1 h at room temperature, followed by washing with wash buffer (500 m*M* NaCl, 10 m*M* Tris-HCl, 2 m*M* EDTA, pH 7.5). The immunoprecipitated sample attached to the immuno-Sepharose beads was incubated in Laemmli sample preparation buffer, prior to 12.5% SDS-PAGE, electrotransfer to nitrocellulose, and immunoblot analysis using specific antibodies to actin (Sigma), fodrin (Santa Cruz Biotechnology Inc., Santa Cruz, CA), vimentin (Sigma, St. Louis, MO), syntaxin 2 (Alomone Labs, Jerusalem, Israel), Ca^{2+}-β3 (Alomone Labs), and Ca^{2+}-α1c (Alomone Labs).

3. Porosome: A New Cellular Structure

Earlier electrophysiological studies on mast cells suggested the existence of fusion pores at the cell PM, which became continuous with the secretory vesicle membrane following stimulation of secretion ***(33)***. AFM has confirmed the existence of the fusion pore or porosome and revealed its structure and dynamics in the exocrine pancreas ***(3,4,7,8)***, neuroendocrine cells ***(5,6)***, and neurons ***(15)***, at near-nanometer resolution and in real time.

Isolated live pancreatic acinar cells in physiological buffer, when imaged with the AFM ***(3,4,7,8)***, reveal at the apical PM, a group of circular "pits" measuring 0.4–1.2 μm in diameter that contain smaller "depressions" (*see* **Fig. 2**). Each depression averages between 100 and 150 nm in diameter, and, typically, three to four depressions are located within a pit. The basolateral membrane of acinar cells is devoid of either pits or depressions. High-resolution AFM images of depressions in live cells further reveal a cone-shaped morphology. The depth of each depression cone measures 15–30 nm. Similarly, growth hormone (GH)-secreting cells of the pituitary gland and chromaffin cells, β-cells of the exocrine pancreas, mast cells, and neurons, possess depressions at their PM, suggesting their universal presence in secretory cells. Exposure of pancreatic acinar cells to a secretagogue (mastoparan) results in a time-dependent increase (20–35%) in depression diameter, followed by a return to resting size on completion of secretion ***(3,4,7,8)*** (*see* **Fig. 3**; *see* Color Plate 16, following p. 274). No demonstrable change in pit size is detected following stimulation of secretion ***(3)***. Enlargement of depression diameter and an increase in its relative depth after exposure to secretagogues correlated with increased secretion. Conversely, exposure of pancreatic acinar cells to cytochalasin B, a fungal toxin that inhibits actin polymerization, results in a 15–20% decrease in depression size and a consequent 50–60% loss in secretion ***(3)***. Results from these studies suggested depressions to be the fusion pores in pancreatic acinar cells. Furthermore, these studies demonstrate the involvement of actin in regulation of both the structure and function of depressions. Analogous to pancreatic acinar cells, examination of resting GH-secreting cells of the pituitary ***(5)*** and

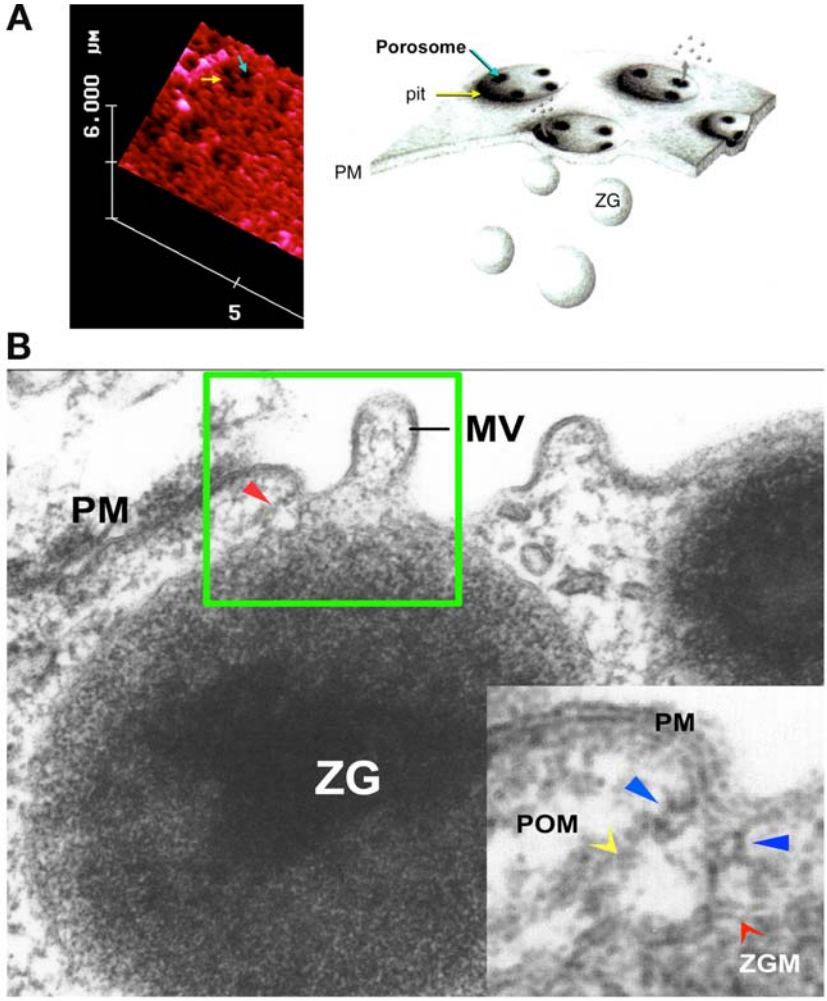

Fig. 2. **(A)** On the far left is an AFM depicting "pits" (arrow to left) and "depressions" within (right arrow), at the PM in live pancreatic acinar cells. On the right is a schematic drawing depicting depressions, at the cell PM, where membrane-bound secretory vesicles dock and fuse to release vesicular contents. **(B)** Electron micrograph depicting a porosome (arrowhead within box) close to a microvillus (MV) at the apical plasma membrane (PM) of a pancreatic acinar cell. Note association of the porosome membrane (POM) and the zymogen granule membrane (ZGM) (a gray arrowhead) of a docked zymogen granule (ZG), the membrane-bound secretory vesicle of exocrine pancreas. Also, a cross-section of the ring at the mouth of the porosome is seen (black arrowheads). (From **ref.** *8*.)

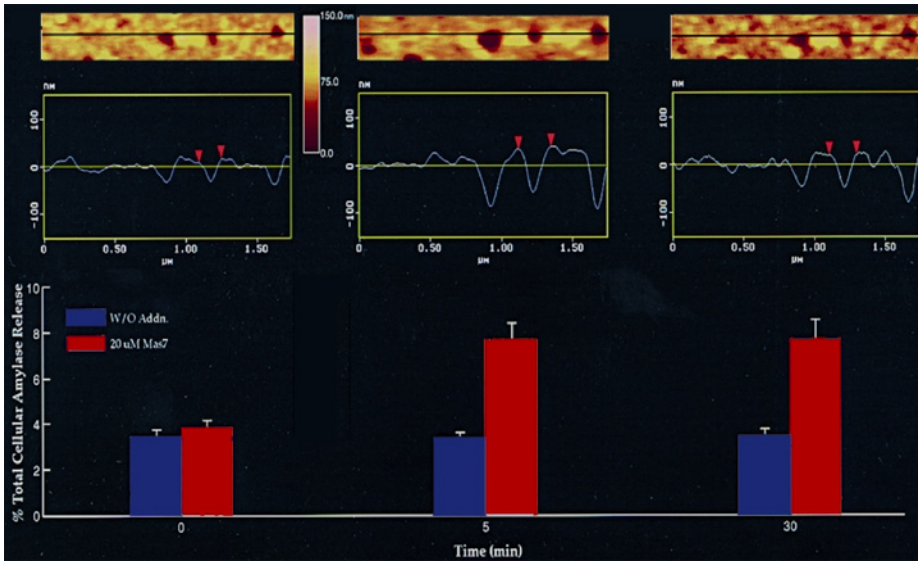

Fig. 3. Dynamics of depressions following stimulation of secretion. The top panel shows a number of depressions within a pit in a live pancreatic acinar cell. The scan line across three depressions in the top panel is represented graphically in the middle panel and defines the diameter and relative depth of the depressions; the middle depressions are represented by arrowheads. The bottom panel represents percent of total cellular amylase release in the presence and absence of the secretagogue Mas 7. Notice an increase in the diameter and depth of depressions, correlating with an increase in total cellular amylase release at 5 min after stimulation of secretion. At 30 min after stimulation of secretion, there is a decrease in diameter and depth of depressions, with no further increase in amylase release over the 5-min time-point. No significant increase in amylase secretion or diameter of depressions was observed in resting acini or those exposed to the nonstimulatory mastoparan analog Mas 17. (*See* Color Plate 16, following p. 274. From **refs.** ***3*** and ***11***.)

chromaffin cells of the adrenal medulla ***(6)*** also reveal the presence of pits and depressions at the cell PM (*see* **Fig. 4**). The presence of porosomes in neurons, β-cells of the endocrine pancreas, and in mast cells have also been demonstrated (*see* **Figs. 4** and **5** [*see* Color Plate 17, following p. 274]) ***(14,15)***. Depressions in resting GH cells measure 154 ± 4.5 nm (mean ± SE) in diameter. Exposure of GH cells to a secretagogue results in a 40% increase in depression diameter (215 ± 4.6 nm; $p < 0.01$) but no appreciable change in pit size. The enlargement of depression diameter during secretion and the known effect that actin depolymerizing agents decrease depression size and inhibit secretion ***(3)*** suggested depressions to be the fusion pores. However, a more direct determination of the function of depressions was required. This was achieved by immuno-

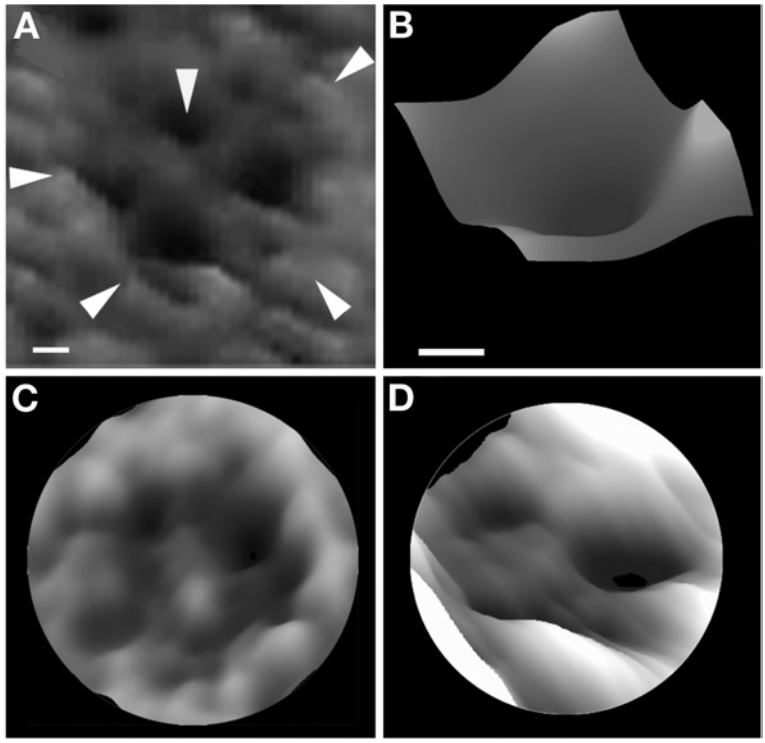

Fig. 4. AFM of depressions or porosomes or fusion pores in live secretory cell of the exocrine pancreas **(A, B)**, the GH-secreting cell of the pituitary **(C)**, and in the chromaffin cell **(D)**. Note the "pit" (arrowheads at the periphery of the structure) with four depressions (arrowhead at 12 o'clock). A high-resolution AFM of a single porosome is shown in B. Bars = 40 nm for A and B. Similarly, AFMs of pororsomes in β-cells of the endocrine pancreas have been demonstrated.

AFM studies. AFM localization at depressions of gold-conjugated antibody to a secretory protein demonstrated secretion to occur through depressions *(4,5)*. The membrane-bound secretory vesicles in exocrine pancreas called ZGs contain the starch-digesting enzyme amylase. Atomic force micrographs demonstrated localization of amylase-specific antibodies tagged with colloidal gold at depressions following stimulation of secretion *(4)* (*see* **Fig. 6**). These studies confirm depressions to be the fusion pores or porosomes in pancreatic acinar cells where membrane-bound secretory vesicles dock and fuse to release vesicular contents. Similarly, in somatotrophs of the pituitary, a gold-tagged GH-specific antibody is found to selectively localize at depressions following stimulation of secretion *(5)*, again identifying depressions in GH cells as fusion pores or porosomes. The porosome at the cytosolic side of the

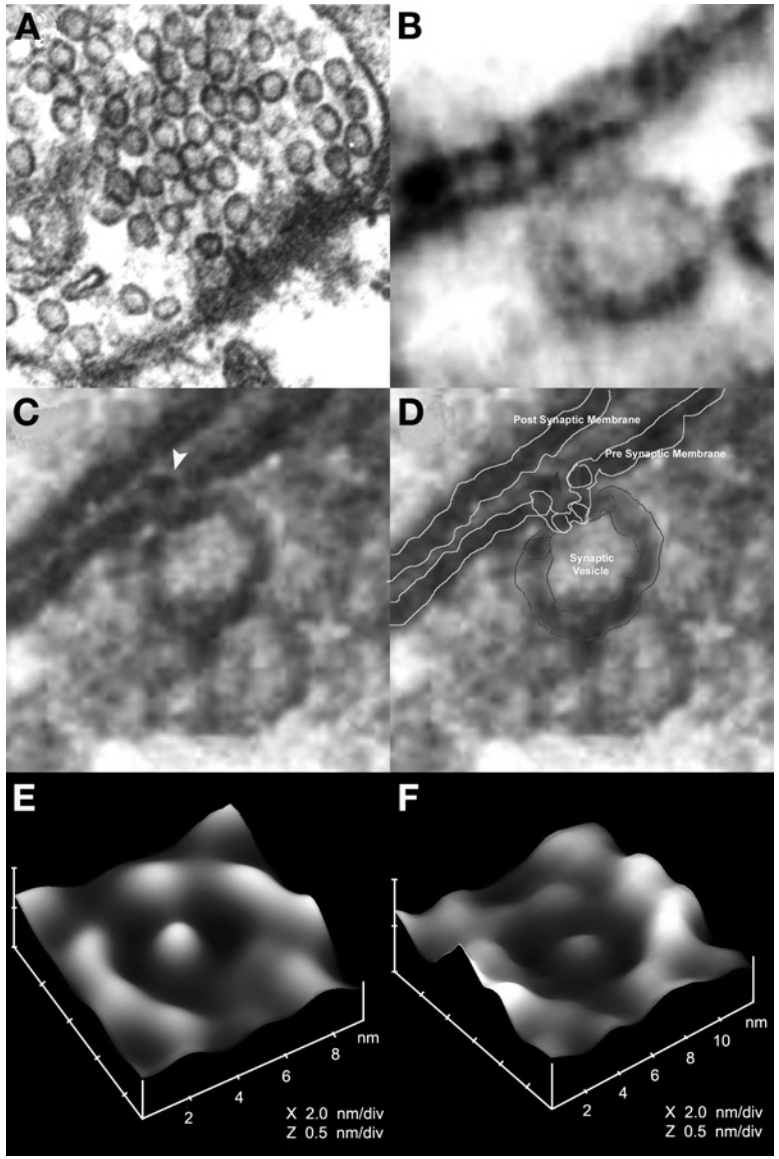

Fig. 5. Electron micrograph of porosomes in neurons. **(A)** Electron micrograph of a synaptosome demonstrating the presence of 40- to 50-nm synaptic vesicles. **(B–D)** Electron micrographs of neuronal porosomes that are 10- to 15-nm cup-shaped structures at the presynaptic membrane (yellow arrowhead), where synaptic vesicles transiently dock and fuse to release vesicular contents. **(E)** AFM of a fusion pore or porosome at the nerve terminal in live synaptosome. **(F)** AFM of isolated neuronal porosome, reconstituted into lipid membrane. (*See* Color Plate 17, following p. 274. From **ref. *15***.)

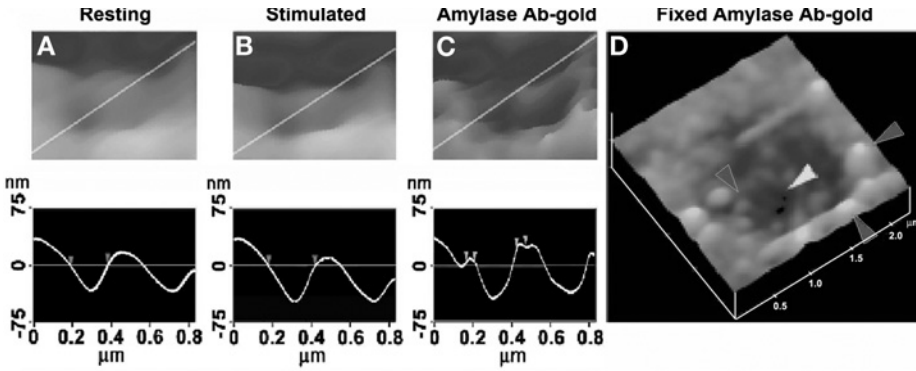

Fig. 6. Depressions are fusion pores or porosomes. Porosomes dilate to allow expulsion of vesicular contents. **(A, B)** AFM and section analysis of a pit and two out of the four fusion pores or porosomes, demonstrating enlargement following stimulation of secretion. Note the section analysis depicting the relative depth and width of the porosome in A through C. **(C)** Exposure of live cells to gold-conjugated-amylase antibody (Ab) results in specific localization of immunogold to the porosome opening. Amylase is one of the proteins within secretory vesicles of the exocrine pancreas. **(D)** AFM of a fixed pancreatic acinar cell, demonstrating a pit and porosomes within, and immunogold-labeling amylase at the site. The dark arrowhead points to immunogold clusters and the white arrowhead points to a porosome. (From **ref. *4*.**)

plasma membrane in the exocrine pancreas ***(7)*** (*see* **Fig. 7**) and in neurons ***(15)*** has also been imaged at near-nanometer resolution in live tissue in buffer.

To determine the morphology of the porosome at the cytosolic side of the cell, pancreatic PM preparations were used. When placed on freshly cleaved mica, isolated PM in buffer tightly adheres to the mica surface, enabling imaging by AFM. The PM preparations reveal scattered circular disks measuring 0.5–1 µm in diameter, with inverted cup-shaped structures within ***(7)***. The inverted cups range in height from 10 to 15 nm. On a number of occasions, ZGs ranging in size from 0.4 to 1 µm in diameter were found associated with one or more of the inverted cups. This suggested the circular disks to be pits and the inverted cups to be fusion pores or porosomes. To determine if the cup-shaped structures in isolated PM preparations are indeed porosomes, immuno-AFM studies were conducted. Because ZGs dock and fuse at the PM to release vesicular contents, it was hypothesized that if porosomes are at these sites, then PM-associated t-SNAREs should localize at the base of porosomes. The t-SNARE protein SNAP-23 has been identified and implicated in secretion from pancreatic acinar cells ***(34)***. A polyclonal monospecific SNAP-23 antibody recognizing a single 23-kDa band in Western blots of pancreatic PM fraction has been used in immuno-AFM studies. When the SNAP-23-specific antibody was

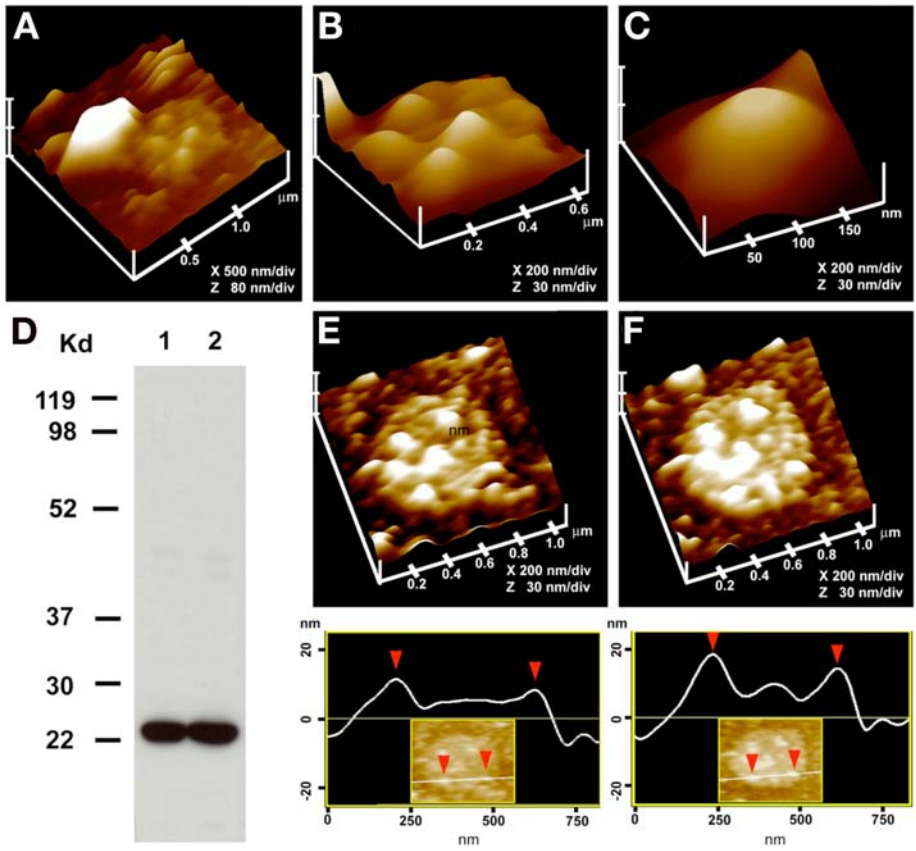

Fig. 7. Morphology of the cytosolic side of the porosome revealed in AFM studies on isolated pancreatic PM preparations. **(A)**. AFM of isolated PM preparation reveals the cytosolic end of a pit with inverted cup-shaped structures, the porosome. Note the 600-nm-diameter ZG at the left-hand corner of the pit. **(B)** Higher magnification of the same pit showing clearly the four to five porosomes within. **(C)** The cytosolic end of a single porosome is depicted in this AFM. **(D)** Immunoblot analysis of 10 µg and 20 µg of pancreatic PM preparations, using SNAP-23 antibody, demonstrates a single 23-kDa immunoreactive band. **(E, F)** The cytosolic side of the PM demonstrating the presence of a pit with a number of porosomes within, shown prior to **(E)** and following addition of the SNAP-23 antibody **(F)**. Note the increase in height of the porosome cone base revealed by section analysis (bottom pannel), demonstrating localization of SNAP-23 antibody at the base of the porosome (From **ref.** *7*).

added to the PM preparation during imaging with the AFM, the antibody selectively localized to the base of the cup-shaped structure, which is the tip of the inverted cup. These results demonstrate that the inverted cup-shaped structures in the isolated PM preparations are the porosomes observed from its cytosolic

side *(7,8)*. Target membrane proteins SNAP-25 and syntaxin (t-SNARE) and secretory vesicle-associated membrane protein (v-SNARE) are part of the conserved protein complex involved in fusion of opposing bilayers *(9,17,18,29)*. Since membrane-bounded secretory vesicles dock and fuse at porosomes to release vesicular contents, this suggested t-SNAREs associate at the porosome complex. It was, therefore, no surprise that the t-SNARE protein SNAP-23, implicated in secretion from pancreatic acinar cells, was located at the tip of the inverted cup (i.e., the base of the porosome) where secretory vesicles dock and fuse.

The structure of the porosome was further demonstrated using transmission electron microscopy (TEM) *(7,8)* (*see* **Fig. 4**). TEM studies confirm the fusion pore to have a cup-shaped structure, with similar dimensions as determined from AFM measurement. Additionally, TEM micrographs reveal porosomes to possess a basketlike morphology, with three lateral and a number of vertically arranged ridges. A ring at the base of the complex is also identified *(7)*. Because porosomes are found to be stable structures at the cell PM, it was hypothesized that if ZGs were to fuse at the base of the structure, it would be possible to isolate ZG-associated porosomes. Indeed, TEM of isolated ZG preparations reveal porosomes associated with docked vesicles *(7,8)*. As observed in whole cells, vertical structures were found to originate from within the porosome complex and appear attached to its membrane. As discussed later in this chapter, studies using full-length recombinant SNARE proteins and artificial lipid membranes demonstrated that t- and v-SNAREs located in opposing bilayers interact in a circular array to form conducting pores *(9)*. Because similar circular structures are observed at the base of the porosome and SNAP-23 immunoreactivity is found to localize at this site, this suggests that the t-SNAREs present at the base of porosomes are possibly arranged in a ring pattern.

3.1. Porosome: Isolation, Composition, and Reconstitution

In the last decade, a number of studies demonstrated the involvement of cytoskeletal proteins in secretion, and some studies implicated direct interaction of cytoskeleton protein with SNAREs *(3,35–39)*. Furthermore, actin and microtubule-based cytoskeleton has been implicated in intracellular vesicle traffic *(3,36)*. Fodrin, which was previously implicated in exocytosis *(35)*, has recently been shown to directly interact with SNAREs *(37)*. Studies demonstrate α-fodrin to regulate exocytosis via its interaction with the t-SNARE syntaxin family of proteins *(37)*. The C-terminal coiled coil region of syntaxin interacts with α-fodrin, a major component of the submembranous cytoskeleton. Similarly, vimentin filaments interact with SNAP23/25 and, hence, are able to control the availability of free SNAP23/25 for assembly of the SNARE complex *(36)*. All of these findings suggested that vimentin, α-fodrin, actin, and

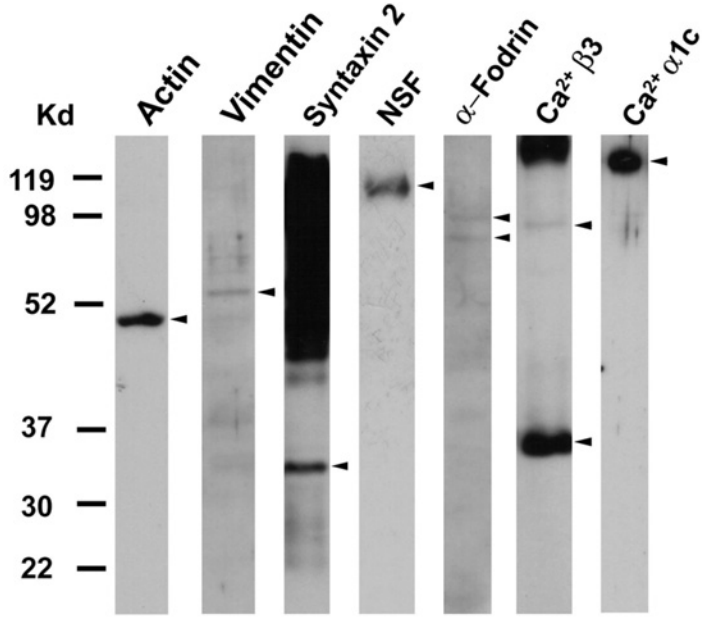

Fig. 8. SNAP-23-associated proteins in pancreatic acinar cells. Total pancreatic homogenate was immunoprecipitated using the SNAP-23-specific antibody. The precipitated material was resolved using 12.5% SDS-PAGE, electrotransferred to nitrocellulose membrane, and then probed using antibodies to a number of proteins. Association of SNAP-23 with syntaxin 2, with cytoskeletal proteins actin, α-fodrin, and vimentin, and calcium channels β3 and α1c, together with the SNARE regulatory protein NSF, is demonstrated (arrow heads). Lanes showing more than one arrowhead suggest the presence of isomers or possible proteolytic degradation of the specific protein. (From **ref. *7***.)

SNAREs might be part of the porosome complex. Additional proteins such as v-SNARE (VAMP or synaptobrevin), synaptophysin, and myosin might associate when the porosome establishes continuity with the secretory vesicle membrane. The globular tail domain of myosin V contains a binding site for VAMP, which is bound in a calcium-independent manner ***(38)***. Further interaction of myosin V with syntaxin requires both calcium and calmodulin. It has been suggested that VAMP acts as a myosin V receptor on secretory vesicles and regulates formation of the SNARE complex ***(38)***. Interaction of VAMP with synaptophysin and myosin V has also been observed ***(39)***. In agreement with these earlier findings, recent studies demonstrated the association of SNAP-23, syntaxin 2, cytoskeletal proteins actin, α-fodrin, and vimentin, and calcium channels β3 and α1c, together with the SNARE regulatory protein NSF, in porosomes ***(7,8)*** (*see* **Fig. 8**). Additionally, chloride-ion channels ClC2 and

ClC3 were also identified as part of the porosome complex *(7,8)*. Isoforms of the various proteins identified in the porosome complex were subsequently demonstrated using 2D-BAC gel electrophoresis *(8,14)*. Three isoforms each of the calcium-ion channel and vimentin were found in porosomes *(8)*. Using yeast 2-hybrid analysis, recent studies confirm the presence and interaction of some of these proteins with t-SNAREs within the porosome complex *(14)*.

The size and shape of the immunoisolated porosome complex was determined in greater detail when examined using both negative staining EM and AFM *(8)*. The images of the immunoisolated porosome obtained by both EM and AFM were superimposable *(8)*. To further test whether the immunoisolated supramolecular complex was indeed the porosome, the complex was reconstituted into artificial liposomes, and the liposome-reconstituted complex examined using TEM *(8)*. Transmission electron micrographs reveal a 150–200-nm cup-shaped basketlike structure as observed for the porosome when coisolated with ZGs. To test if the reconstituted porosome complex was functional, purified porosomes were reconstituted into lipid membranes in an electrophysiological bilayer setup (EPC9) and challenged with isolated ZGs. Both the electrical activity of the reconstituted membrane as well as the transport of vesicular contents from the cis to the trans compartment were monitored. Results of these experiments demonstrate that the lipid membrane-reconstituted porosomes are functional supramolecular complexes (*see* **Figs. 9** and **10**) *(8)*. ZGs fused with the porosome-reconstituted bilayer, as demonstrated by an increase in capacitance and conductance and in a time-dependent release of the ZG enzyme amylase from the cis to the trans compartment of the bilayer chamber. Amylase is detected using immunoblot analysis of the buffer in the cis and trans chambers, using a previously characterized amylase-specific antibody *(4)*. As observed in immunoblot assays of isolated porosomes, chloride channel activities are also detected within the reconstituted porosome complex. Further, the chloride channel inhibitor DIDS was found to inhibit current activity in the porosome-reconstituted bilayer. In summary, these studies demonstrate that the porosome in the exocrine pancreas is a 100- to 150-nm-diameter supramolecular cup-shaped lipoprotein basket at the cell PM, where membrane-bound secretory vesicles dock and fuse to release vesicular contents. Similar studies have now been performed in neurons, demonstrating both the structural (*see* **Fig. 5E,F**) and functional reconstitution of the isolated neuronal porosome complex. The biochemical composition of the neuronal porosome has also been determined *(15)*.

3.2. Molecular Understanding of Cell Secretion

Fusion pores or porosomes are present in all secretory cells examined. From exocrine, to endocrine, to neuroendocrine, to neurons, where membrane-bound

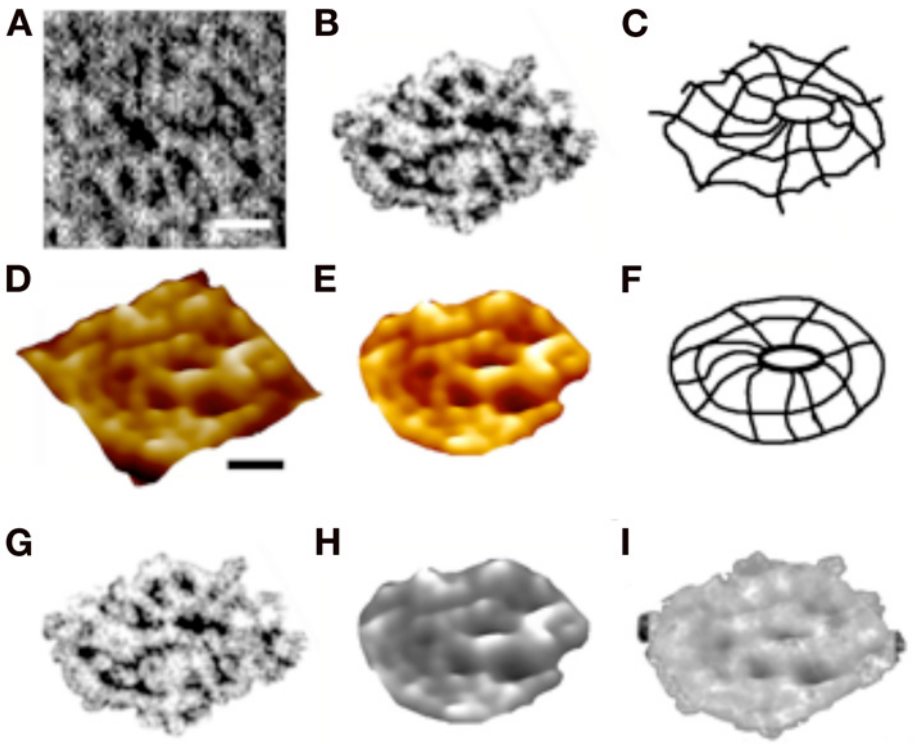

Fig. 9. Negatively stained EM and AFM of the immunoisolated porosome complex. **(A)** Negatively stained EM of an immunoisolated porosome complex from solubilized pancreatic plasma membrane preparations, using a SNAP-23-specific antibody. Note the 3 rings and the 10 spokes that originate from the inner smallest ring. This structure represents the protein backbone of the porosome complex, because the three rings and the vertical spikes are observed in EMs of cells and porosome coisolated with ZGs. Bar = 30 nm. **(B)** The EM of the fusion pore complex, cut out from **(A)**, and **(C)** an outline of the structure is presented for clarity. **(D–F)** AFM of the isolated porosome complex in near physiological buffer. Bar = 30 nm. Note the structural similarity of the complex, imaged both by EM **(G)** and AFM **(H)**. The EM and AFM micrographs are superimposable **(I)**.

secretory vesicles dock and transiently fuse to expel vesicular contents. Porosomes in pancreatic acinar or GH-secreting cells are cone-shaped structures at the plasma membrane, with a 100- to 150-nm-diameter opening. Membrane-bound secretory vesicles ranging in size from 0.2 to 1.2 μm in diameter dock and fuse at porosomes to release vesicular contents. Following fusion of secretory vesicles at porosomes, only a 20–35% increase in porosome diameter is demonstrated. It is therefore reasonable to conclude that secretory vesicles “transiently” dock and fuse at the site. In contrast to

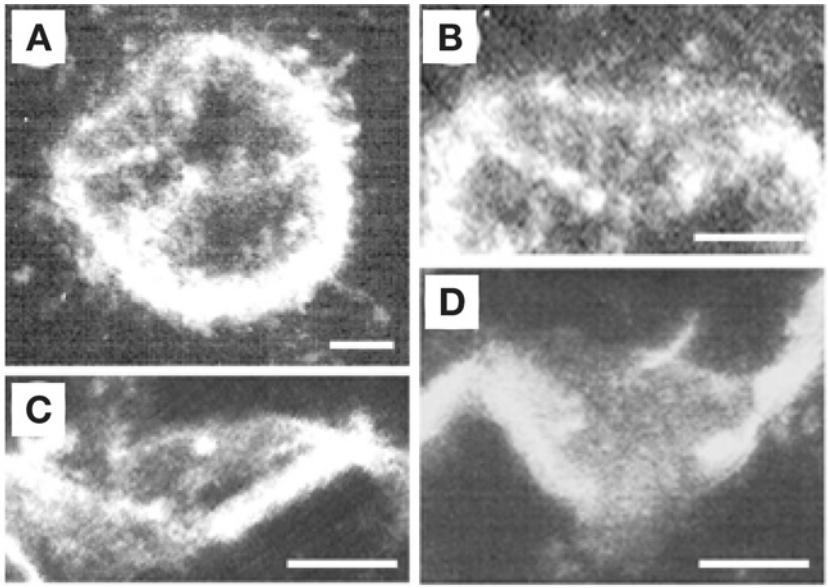

Fig. 10. Electron micrographs of liposome reconstituted porosome from pancreas demonstrating a cup-shaped basketlike morphology. **(A)** A 500-nm vesicle with an incorporated porosome is shown. Note the spokes in the complex. The reconstituted complex at greater magnification is shown in **B–D** Bar = 100 nm.

accepted belief, if secretory vesicles were to completely incorporate at porosomes, the PM structure would distend much wider than what is observed. Furthermore, if secretory vesicles were to completely fuse at the plasma membrane, there would be a loss in vesicle number following secretion. Examination of secretory vesicles within cells before and after secretion demonstrates that the total number of secretory vesicles remains unchanged following secretion *(10,26)*. However, the number of empty and partially empty vesicles increases significantly, supporting the occurrence of transient fusion. Earlier studies on mast cells also demonstrated an increase in the number of spent and partially spent vesicles following stimulation of secretion, without any demonstrable increase in cell size. Similarly, secretory granules are recaptured largely intact after stimulated exocytosis in cultured endocrine cells *(22)*. Other supporting evidence favoring transient fusion is the presence of neurotransmitter transporters at the synaptic vesicle membrane. These vesicle-associated transporters would be of little use if vesicles were to fuse completely at the plasma membrane to be compensatorily endocytosed at a later time. In further support, a recent study reports that single synaptic vesicles fuse transiently and successively without loss of vesicle identity *(23)*. Although the

fusion of secretory vesicles at the cell PM occurs transiently, complete incorporation of membrane at the cell plasma membrane would occur when cells need to incorporate signaling molecules like receptors, second messengers, or ion channels. The discovery of the porosome and an understanding of the molecular mechanism of membrane fusion and the swelling of secretory vesicles required for expulsion of vesicular contents provide an understanding of secretion and membrane fusion in cells at the molecular level. These findings have prompted many laboratories to work in the area and further confirm these findings. Thus, the porosome is a supramolecular structure universally present in secretory cells, from the exocrine pancreas to the neurons, and in the endocrine to neuroendocrine cells, where membrane-bound secretory vesicles transiently dock and fuse to expel vesicular contents. Hence, the secretory process in cells is a highly regulated event, orchestrated by a number of ions and biomolecules.

Acknowledgment

This work was supported by grants DK-56212 and NS-39918 from the National Institutes of Health (BPJ).

References

1. Hörber, J. K. H. and Miles, M. J. (2003) Scanning probe evolution in biology. *Science* **302**, 1002–1005.
2. Anderson, L. L. (2004) Discovery of a new cellular structure—the porosome: elucidation of the molecular mechanism of secretion. *Cell Biol. Int.* **28**, 3–5.
3. Schneider, S. W., Sritharan, K. C., Geibel, J. P., Oberleithner, H., and Jena, B. P. (1997) Surface dynamics in living acinar cells imaged by atomic force microscopy: identification of plasma pembrane structures involved in exocytosis. *Proc. Natl. Acad. Sci. USA* **94**, 316–321.
4. Cho, S. J., Quinn, A. S., Stromer, M. H., et al. (2002) Structure and dynamics of the fusion pore in live cells. *Cell Biol. Int.* **26**, 35–42.
5. Cho, S. J., Jeftinija, K., Glavaski, A., Jeftinija, S., Jena, B. P., and Anderson, L. L. (2002) Structure and dynamics of the fusion pores in live GH-secreting cells revealed using atomic force microscopy. *Endocrinology* **143**, 1144–1148.
6. Cho, S. J., Wakade, A., Pappas, G. D., and Jena, B. P. (2002) New structure involved in transient membrane fusion and exocytosis. *Ann. New York Acad. Sci.* **971**, 254–256.
7. Jena, B. P., Cho, S. J., Jeremic, A., Stromer, M. H., and Abu-Hamdah, R. (2003) Structure and composition of the fusion pore. *Biophys. J.* **84**, 1337–1343.
8. Jeremic, A., Kelly, M., Cho, S. J., Stromer, M. H., and Jena, B. P. (2003) Reconstituted fusion pore. *Biophys. J.* **85**, 2035–2043.
9. Cho, S. J., Kelly, M., Rognlien, K. T., Cho, J., Hoerber, J. K. H., and Jena, B. P. (2002) SNAREs in opposing bilayers interact in a circular array to form conducting pores. *Biophys. J.* **83**, 2522–2527.

10. Cho, S. J., Cho, J., and Jena, B. P. (2002) The number of secretory vesicles remains unchanged following exocytosis. *Cell Biol. Int.* **26**, 29–33.
11. Jena, B. P. (2002) Fusion pore in live cells. *NIPS* **17**, 219–222.
12. Jena, B. P. (2003) Fusion pore: structure and dynamics. *J. Endocrinol.* **176**, 169–174.
13. Jena, B. P. (1997) Exocytotic fusion: total or transient. *Cell Biol. Int.* **21**, 257–259.
14. Jena, B. P. (2004) Discovery of the porosome: revealing the molecular mechanism of secretion and membrane fusion in cells. *J. Cell Mol. Med.* **8**, 1–21.
15. Cho, W. J., Jeremic, A., Rognlien, K. T., et al. (2004). Structure, isolation, composition and reconstitution of the neuronal fusion pore. *Cell Biol. Int.* **28**, 699–708. (published on-line August 25, 2004).
16. Kelly, M., Cho, W. J., Jeremic, A., Abu-Hamdah, R., and Jena, B. P. (2004). Vesicle swelling regulates content expulsion during secretion. *Cell Biol. Int.* **28**, 709–716 (published on-line August 25, 2004).
17. Jeremic, A., Kelly, M., Cho, W. J., Cho, S. J., Horber, J. K. H., and Jena, B. P. (2004) Calcium drives fusion of SNARE-apposed bilayers. *Cell Biol. Int.* **28**, 19–31 (published on-line 2003).
18. Jeremic, A., Cho, W. J., and Jena, B. P. (2004) Membrane fusion: what may transpire at the atomic level. *J. Biol. Phys. Chem.* **4**, 139–142.
19. Jena, B. P., Schneider, S. W., Geibel, J. P., Webster, P., Oberleithner, H., and Sritharan, K. C. (1997) G_i regulation of secretory vesicle swelling examined by atomic force microscopy. *Proc. Natl. Acad. Sci. USA* **94**, 13,317–13,322.
20. Cho, S. J., Sattar, A. K., Jeong, E.-H., et al. (2002) Aquaporin 1 regulates GTP-induced rapid gating of water in secretory vesicles. *Proc. Natl. Acad. Sci. USA* **99**, 4720–4724.
21. Abu-Hamdah, R., Cho, W. J., Cho, S. J., et al. (2004) Regulation of the water channel aquaporin-1: isolation and reconstitution of the regulatory complex. *Cell Biol. Int.* **28,** 7–17. (published on-line 2003).
22. Taraska, J. W., Perrais, D., Ohara-Imaizumi, M., Nagamatsu, S., and Almers, W. (2003) Secretory granules are recaptured largely intact after stimulated exocytosis in cultured endocrine cells. *Proc. Natl. Acad. Sci. USA* **100**, 2070–2075.
23. Aravanis, A. M., Pyle, J. L., and Tsien, R. W. (2003) Single synaptic vesicles fusing transiently and successively without loss of identity. *Nature* **423**, 643–647.
24. Tojima, T., Yamane, Y., Takagi, H., et al. (2000) Three-dimensional characterization of interior structures of exocytotic apertures of nerve cells using atomic force microscopy. *Neuroscience* **101**, 471–481.
25. Thorn, P., Fogarty, K. E., and Parker, I. (2004) Zymogen granule exocytosis is characterized by long fusion pore openings and preservation of vesicle lipid identity. *Proc. Natl. Acad. Sci. USA* **101**, 6774–6779.
26. Lee, J. S., Mayes, M. S., Stromer, M. H., Scanes, C. G., Jeftinija, S., and Anderson, L. L. (2004) Number of secretory vesicles in growth hormone cells of the pituitary remains unchanged after secretion. *Exp. Biol. Med.* **229**, 291–302.
27. Fix, M., Melia, T. J., Jaiswal, J. K., et al. (2004) Imaging single membrane fusion events mediated by SNARE proteins. *Proc. Natl. Acad. Sci. USA* **101**, 7311–7316.

28. Binnig, G., Quate, C. F., and Gerber, C. H. (1986) Atomic force microscope. *Phys. Rev. Lett.* **56**, 930–933.
29. Weber, T., Zemelman, B. V., McNew, J. A., et al. (1998) SNAREpins: minimal machinery for membrane fusion. *Cell* **92**, 759–772.
30. Alexander, S., Hellemans, L., Marti, O., Schneir, J., Elings, V., and Hansma, P. K. (1989) An atomic resolution atomic force microscope implemented using an optical lever. *J. Appl. Phys.* **65**, 164–167.
31. Jeong, E-H., Webster, P., Khuong, C. Q., Sattar, A. K. M. A., Satchi, M., and Jena, B. P. (1998) The native membrane fusion machinery in cells. *Cell Biol. Int.* **22**, 657–670.
32. Thoidis, G., Chen, P., Pushkin, A. V., et al. (1998) Two distinct populations of synaptic-like vesicles from rat brain. *Proc. Natl. Acad. Sci. USA* **95**, 183–188.
33. Monck, J. R., Oberhauser, A. F., and Fernandez, J. M. (1995) The exocytotic fusion pore interface: a model of the site of neurotransmitter release. *Mol. Membr. Biol.* **12**, 151–156.
34. Gaisano, H. Y., Sheu, L., Wong, P. P., Klip, A., and Trimble, W. S. (1997) SNAP-23 is located in the basolateral plasma membrane of rat pancreatic acinar cells. *FEBS Lett.* **414**, 298–302.
35. Bennett, V. (1990) Spectrin-based membrane skeleton: a multipotential adaptor between plasma membrane and cytoplasm. *Physiol. Rev.* **70**, 1029–1065.
36. Faigle, W., Colucci-Guyon, E., Louvard, D., Amigorena, S., and Galli, T. (2000) Vimentin filaments in fibroblasts are a reservoir for SNAP-23, a component of the membrane fusion machinery. *Mol. Biol. Cell.* **11**, 3485–3494.
37. Goodson, H. V., Valetti, C., and Kreis, T. E. (1997) Motors and membrane traffic. *Curr. Opin. Cell Biol.* **9**, 18–28.
38. Nakano, M., Nogami, S., Sato, S., Terano, A., and Shirataki, H. (2001) Interaction of syntaxin with α-fodrin, a major component of the submembranous cytoskeleton. *Biochem. Biophys. Res. Commun.* **288**, 468–475.
39. Ohyama, A., Komiya, Y., and Igarashi, M. (2001) Globular tail of myosin-V is bound to vamp/synaptobrevin. *Biochem. Biophys. Res. Commun.* **280**, 988–991.